

Communication

Highly Photostable and pH–Sensitive Nanosensors

Zhenzhen Lin ¹, Fang Hu ², Gang He ^{3,*}, Youjun Yang ², Yujun Liao ⁴, Xiao Luo ^{5,*} and Xu-Dong Wang ^{1,*}¹ Department of Chemistry, Human Phenome Institute, Fudan University, Shanghai 200438, China² Shanghai Frontiers Science Center of Optogenetic Techniques for Cell Metabolism, State Key Laboratory of Bioreactor Engineering, Shanghai Key Laboratory of Chemical Biology, School of Pharmacy, East China University of Science and Technology, Shanghai 200237, China³ State Key Laboratory for Strength and Vibration of Mechanical Structures, Frontier Institute of Science and Technology, Xi'an Jiaotong University, Xi'an 710054, China⁴ Department of Neurosurgery, Huashan Hospital of Fudan University, 12 Middle Wulumuqi Road, Shanghai 200040, China⁵ Shanghai Engineering Research Center of Molecular Therapeutics and New Drug Development, School of Chemistry and Molecular Engineering, East China Normal University, Dongchuan Road 500, Shanghai 200241, China

* Correspondence: ganghe@mail.xjtu.edu.cn (G.H.); xluo@ecnu.edu.cn (X.L.); wangxudong@fudan.edu.cn (X.-D.W.)

Abstract: Determination of pH values has a vital influence in many chemical and biological processes. To accurately determine pH values, we fabricated a highly photostable ratiometric fluorescent pH–sensitive nanosensor by staining the core of mesoporous silica nanoparticle with a rhodol dye and chemically labelling its outer shell with a rhodamine derivative dye. The two dyes possess opposite pH–responding directions, which increases the band of the signal change. There is a nine–fold change in fluorescence intensity ratios when the solution pH changes from 3.0 and 9.0. Meanwhile, the nanosensors displayed yellowish emission in low pH value, orange emission in mid pH value, and reddish emission in high pH value, which can be readily inspected by bare eyes. Last but not least, excellent photostability and reversibility features make the nanosensors useful for the continuous measuring of pH with high accuracy.

Keywords: ratiometric nanosensors; pH sensing; dual probe; silica nanoparticles



Citation: Lin, Z.; Hu, F.; He, G.; Yang, Y.; Liao, Y.; Luo, X.; Wang, X.-D.

Highly Photostable and pH–Sensitive Nanosensors.

Chemosensors **2022**, *10*, 354.

<https://doi.org/10.3390/chemosensors10090354>

chemosensors10090354

Academic Editor: Marco Pisco

Received: 2 July 2022

Accepted: 23 August 2022

Published: 26 August 2022

Publisher's Note: MDPI stays neutral with regard to jurisdictional claims in published maps and institutional affiliations.



Copyright: © 2022 by the authors. Licensee MDPI, Basel, Switzerland. This article is an open access article distributed under the terms and conditions of the Creative Commons Attribution (CC BY) license (<https://creativecommons.org/licenses/by/4.0/>).

1. Introduction

The pH value is one of the most measured chemical parameters in industry, agriculture, environmental science, and even in daily life. Efforts have been devoted since the very beginning of modern science to establishing methods for measuring pH, including pH test strips via visual inspection, pH glass electrode and other electrical methods, optical methods, and magnetic methods [1]. Among these approaches, pH sensing based on changes in fluorescence properties of fluorophores attracts most attention, due to its excellent robustness in contactless sensing, high sensitivity, high selectivity, and non–invasiveness as well as easy miniaturization [2].

The fluorophores have two photophysical properties that can be explored for sensing changes in pH, the fluorescence intensity and lifetime. The former can be measured via simple instrumentation, and a device can be designed that is as small as a USB stick [2]. However, fluorescence intensity varies widely according to instrumentation, probe concentration, dye photobleaching, and light variations [3]. In contrast, fluorescence lifetime is immune to the above–mentioned interferences. Unfortunately, lifetime measurement requires more sophisticated devices [2], which is expensive and not easy to be miniaturized into portable devices.

In order to overcome these limitations, a dual–wavelength referencing approach is developed, which shows obvious advantages in accuracy, simplicity of device, and

low cost. Probes for dual wavelength referencing can be categorized into two major groups: (1) single fluorophore which possesses dual excitation or emission bands; (2) two fluorophores used as ratiometric pairs. For the former, influences of dye concentration and photobleaching can be eliminated since both fluorescence emissions are emitted from the same fluorophore. Trisodium salt of 8-hydroxyl-1,3,6-pyrene trisulfonic acid (HPTS) [4], seminaphthorhodafluor (SNARF) [5], and pHluorin [6] have been reported for ratiometric pH measurement. However, this kind of fluorophores are rare and most of them have limited measurement range. Although it is possible to covalently link two fluorophores into one molecule, difficulties and complication in synthesis and purification hinder their development. Hence, it is no surprise to witness that only limited examples were reported to date, involving phenanthro[9,10-d]imidazole with vinylpyridine [7], phenothiazine with hydrazine [8], fluorescein isothiocyanate (FITC) with cyanine [9], fluorescein with rhodamine [10], and iminocoumarin with salicylic aldehyde [11].

As a result, immobilization of two fluorophores into one matrix becomes the main stream in developing ratiometric pH sensors. Generally, there are three different combinations: (1) sensors with one pH-sensitive probe and one pH-insensitive probe; (2) sensors with two pH-sensitive probes that have the same pH-responding direction; and (3) sensors with two pH-sensitive probes that have opposite pH-responding directions. Obviously, the third combination will have the most substantial signal change. The more substantial the signal change is, the higher the sensitivity will be, and the more accurate the measurement will be. Until now, many ratiometric pH sensors have been reported. However, sensors of the third combination are limited, and those with single wavelength excitation mode are even fewer. The reason is that single wavelength excitation mode could undoubtedly simplify the operation and avoid systematic error caused by switching excitation wavelengths, but it brings difficulty in the design and selection of the fluorophore pairs. On the other hand, it should be noted that there should be no significant difference in the photostability of the fluorophore pairs for the reason that different photobleaching rate will bring the drift of fluorescence ratio over time and error in long-time measurement. A certain amount of literature uses FITC as one of the ratiometric pairs [9,10,12]. However, Peng et al. have reported that FITC has poor photostability and its photostability is different from ruthenium (II) complexes [13]. Moreover, data on the photostability of ratiometric pH sensors were frequently lacking in the previous studies. Therefore, pH-sensitive nanosensors with better properties (high photostability and accuracy) are strongly preferred.

In this study, we have constructed a highly photostable pH-sensitive nanosensors based on two probes—pHD and pHI. Mesoporous silica nanoparticles are applied as the nanosensors to carry the probes. Opposite pH-responding directions and single wavelength excitation mode make the nanosensors superior in accuracy and simplicity of measurement. The nanosensors are able to reversibly measure pH in the range of 3.0–9.0 with high sensitivity and excellent stability.

2. Materials and Methods

2.1. Reagents and Instruments

N,N'-dicyclohexylcarbodiimide (DCC), N-hydroxysuccinimide (NHS), aminopropyltriethoxysilane (APTES), and triethylamine (TEA) were purchased from TCI (www.tcichemicals.com (accessed on 15 July 2022)). (1-Hexadecyl)trimethylammonium bromide was bought from Alfa Aesa (www.thermofisher.com (accessed on 15 July 2022)). Dimethylsulfoxide (DMSO) were obtained from Tansoole (www.tansoole.com (accessed on 15 July 2022)). Tetraethyl orthosilicate (TEOS) were purchased from Sigma-Aldrich (www.sigmaaldrich.com (accessed on 15 July 2022)). The dyes pHD and pHI were synthesized according to literature [14,15]. Britton-Robinson (BR) buffer solution (100 mM) was prepared from boric acid, phosphoric acid, acetic acid, and sodium hydroxide, and the pH of buffer solution was adjusted using 12.0 M hydrochloric acid and 2.0 M sodium hydroxide solution. All chemicals were of analytical grade and used as received without further purification. Deionized (DI) water was used throughout all experiments.

Transmission electron microscopic images of samples were obtained using a field emission transmission electron microscope (FEI Tecnai G2 F20 S–Twin, maximum voltage of 200 kV) and a transmission electron microscope (Hitachi HT7700 Exalens, operating at 120 kV). Fluorescence spectra was recorded using a fluorescence spectrophotometer (Hitachi F–7000). The excitation and emission slit width of the spectrometer were both set at 10 nm. The pH values of BR buffers were measured using a digital pH electrode (Ohaus STARTER 3100), the electrode was calibrated using certificated pH standards (4.00, 7.00 and 10.00) at room temperature before use.

2.2. Preparation of the Ratiometric pH Nanosensors

2.2.1. Preparation of pHI–Silane

DCC (0.95 mg, 4.5 μmol), NHS (0.53 mg, 4.5 μmol) and pHI (0.73 mg, 1.5 μmol) were dissolved in 270 μL DMSO and stirred for 12 h. Then APTES (7.5 μmol , 1.8 μL) was introduced into the mixture and reacted for 12 h. All solutions were protected in dried Argon atmosphere and temperature was controlled at 30 $^{\circ}\text{C}$ in the thermostank.

2.2.2. Preparation of pHD–Silane

The stock solution of pHD was prepared by dissolving the dye in dried DMSO at a concentration of 10.0 mM. Firstly, DCC (0.63 mg, 3 μmol) and NHS (0.71 mg, 6 μmol) were dissolved in 320 μL DMSO. Then 30 μL pHD stock solution (10 mM, 0.3 μmol) was added and kept stirring for 3 h. Finally, 36 μL absolute ethanol containing 1.0% *v/v* APTES (1.5 μmol) was added, and the solution was continuously stirred for 12 h. All solutions were also protected in dried Argon atmosphere and temperature was controlled at 30 $^{\circ}\text{C}$ in the thermostank.

2.2.3. Immobilizing pHI Inside Mesoporous Silica Nanoparticles (mSiNPs)

Synthesis of pHI–doped mesoporous silica nanoparticles was adapted from the literature [16]. CTAB (140 mg) and ddH₂O (3.7 mL) was added into a 25 mL flask and the formed mixture was stirred for 10 min. Subsequently, 525 μL ethanol was added to the mixture and kept stirring for 10 min. Then, TEA (206 μL) was added and the flask was immersed into an oil bath which was preheated to 60 $^{\circ}\text{C}$. After stirring for 10 min, TEOS (300 μL) and pHI–silane (272 μL) was added dropwise into the mixture and kept under stirring for 2 h. Next, TEOS (50 μL) was added and kept under stirring for 1 h. Finally, the flask was immersed in an oil bath at 30 $^{\circ}\text{C}$ for 12 h. The mixture was centrifuged at $17,000\times g$ for 10 min and washed with 95% ethanol for five times. The obtained nanoparticles (denoted as pHI@mSiO₂) was redispersed in 95% ethanol at a concentration of 10.0 mg·mL^{−1}.

2.2.4. Immobilizing pHD on the Surface of mSiNPs

pHD–silane (386 μL) was added to pHI@mSiO₂ solution (1.0 mL, 10.0 mg·mL^{−1}) and kept under stirring at 30 $^{\circ}\text{C}$ for 24 h. The mixture was centrifuged at $17,000\times g$ for 10 min, and washed with 95% ethanol for three times. The ratiometric pH nanosensors were redispersed in 1.0 mL 95% ethanol.

2.2.5. In Vitro Fluorescence Measurement

The dyes pHD and pHI were respectively dispersed in 100 mM Britton–Robinson buffer at a concentration of 1 μM and 10 μM . The ratiometric pH–sensitive nanosensors were dispersed in 100 mM Britton–Robinson buffer at a concentration of 1.0 mg·mL^{−1}. The excitation wavelength was at 545 nm. The slit widths of excitation and the emission on the spectrometer were set at 10 nm.

2.2.6. Analysis of the pH Response

For a fluorescence pH probe, the pH value of the solution can be calculated by Equation (1) according to Henderson–Hasselbalch equation

$$\text{pH} = \text{pK}_a + \lg \frac{[\text{A}^-]}{[\text{HA}]} \quad (1)$$

Equation (1) can be rewritten in the form of Equation (2) when fluorescence intensity is used. [17] In Equation (2), I_{\max} and I_{\min} are the fluorescence intensity I at the highest and lowest pH values, respectively.

$$\text{pH} = \text{pK}_a + \lg \frac{I_{\max} - I}{I - I_{\min}} \quad (2)$$

For ratiometric fluorescent indicators, the dependence of fluorescence intensity ratio on pH can be described by the two–state model of fluorophore protonation according to Equation (3) [18,19]

$$R = R_0 \left(\frac{R_f + 10^{\text{pK}_a - \text{pH}}}{1 + 10^{\text{pK}_a - \text{pH}}} \right) \quad (3)$$

3. Results

In order to create a highly photostable pH–sensitive nanosensor, the selection of pH probes is essential. We designed two pH–sensitive probes with analogous conjugation system xanthene (Figure 1), which contributes to the overlap of their absorption spectra (Figure 2a). Hence, the two probes could be simultaneously excited at a single wavelength (545 nm) or a 532 nm commercial laser, conducting to more simple operation and more accurate measurement results as mentioned above. When excited at 545 nm, the emission of pHD and pHI maximized at 575 nm and 650 nm, respectively (Figure 2b), which separated distinctly from each other.

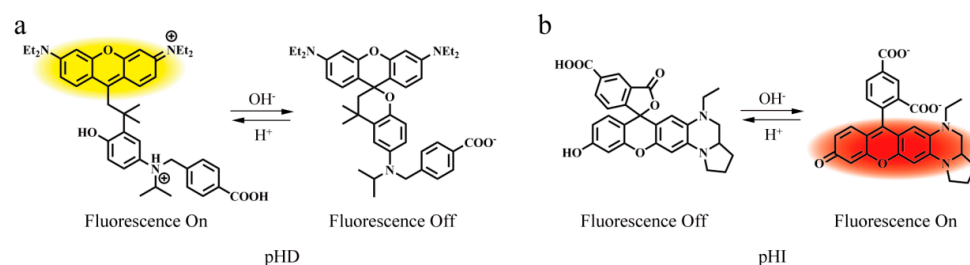


Figure 1. Structure and proposed mechanism of (a) pHD and (b) pHI.

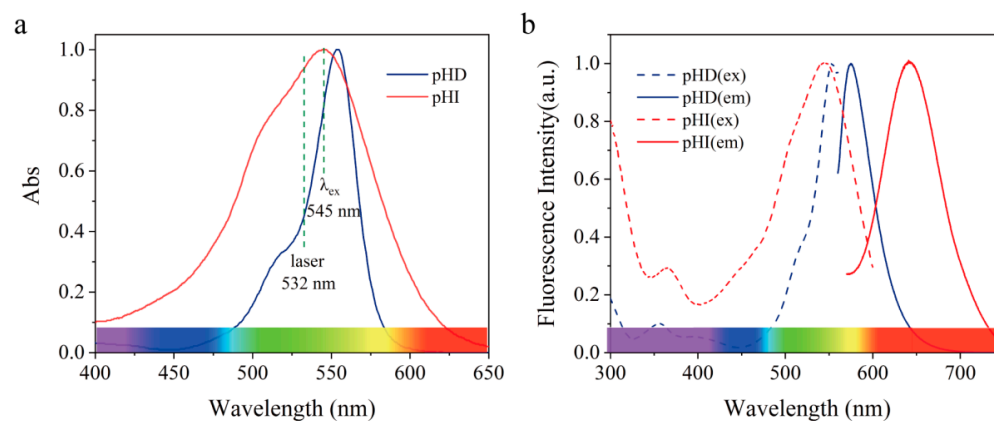


Figure 2. (a) Normalized absorption spectra of pHD and pHI. (b) Normalized excitation and emission spectra of pHD and pHI. pHD and pHI are separately dispersed in BR buffer solution at pH 3.0 and 9.0.

As shown in Figure 3a,b, the two probes presented opposite pH–responding directions. When solution pH increases from 3.0 to 9.0, a decrease in emission intensity of pHD and an increase in emission intensity of pHI were observed. The pH–dependent fluorescence intensities of the two probes are modulated via the mechanisms of intramolecular charge transfer and the conjugation disruption/restoration (Figure 1). As for pHD, the phenolic hydroxyl group is tethered to the meso methine carbon of a rhodamine scaffold via an ether bridge while in pHI molecule, the phenolic hydroxyl group is part of the electronic *push–pull* system of the rhodol fluorochrome. Under the acidic condition, pHD undergoes a protonation–induced ring–opening and restoration of the *push–pull* electronic backbone and exhibits a fluorescence turn–on. Under the same condition, pHI predominantly adopts the non–fluorescent ring–closed lactone, and the fluorescence is weak. Under the basic condition, deprotonation of the phenolic hydroxyl group of pHD induces the ring–closing leading to the conjugation disruption and the weak fluorescence. Under the same condition, deprotonation of the phenolic hydroxyl group of pHI induces the ring–opening of the lactone and the formation of the bright rhodol fluorophore. The relationship between fluorescence intensity and pH was shown in Figure 3c, indicating the calculated pK_a of pHD and pHI was 4.3 and 6.8, respectively.

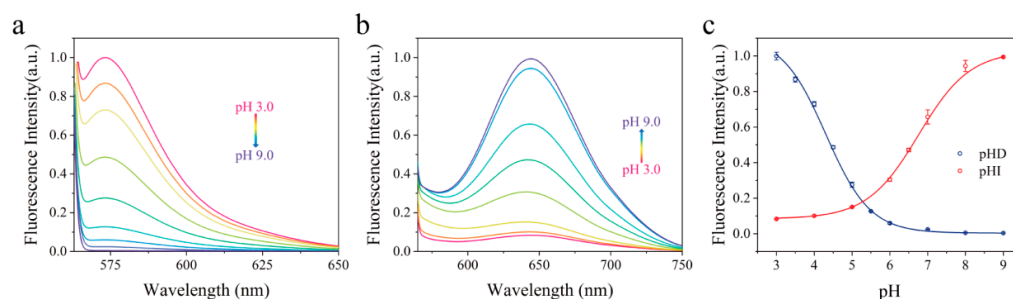


Figure 3. Normalized fluorescence emission spectra of (a) pHD and (b) pHI in BR buffer solution at different pHs. (c) pH–dependent emission intensity of pHD at 575 nm and pHI at 650 nm.

In order to create highly photostable pH–sensitive nanosensors, mesoporous silica nanoparticles (mSiNPs) were selected as the carrier for the two probes. mSiNPs have highly porous structure and large specific surface area, and their surface can be easily functionalized with well–established silane technique, contributing to large amount of dyes immobilized at desired locations and high brightness. In addition, mSiNPs are not only easy to prepare, but are also optically transparent and they have excellent mechanical stability. The synthesis of nanosensors have been optimized using different methods (Supporting Information, Figures S1 and S2). Both pHD and pHI were modified with free carboxyl group, so that they could be chemically linked on the inner and outer surface of mSiNPs at an optimized molar ratio (Table S1 and Figure S3 in the Supporting Information).

Figure 4a showed the structure of constructed nanosensors, whose core was stained with pHI (red), and its outer shell was chemically labelled with pHD (yellow). TEM analysis revealed the nanosensors had a mesoporous structure (Figure 4b) and the average diameter of the nanosensors was 47.5 ± 4.8 nm (Figure 4c). The mesoporous structure is beneficial to proton diffusion and interaction with both pH–sensitive probes.

Figure 5a showed the fluorescence spectra of nanosensors in the media at pH 3.0–9.0 upon excitation at 545 nm. The nanosensors emitted two characteristic emission bands centered at 570 nm and 630 nm, corresponding to the emission of pHD and pHI, respectively. Both probes retained their pH responding characters after immobilization. The emission at 570 nm decreased and that at 630 nm increased as pH elevated, with apparent color changed from yellowish red to dense red (the insert of Figure 5a). By plotting the ratio of intensities at 570 nm and 630 nm ($I_{570\text{ nm}}/I_{630\text{ nm}}$) with pH (Figure 5b), there is a nearly nine–fold signal variation (from 5.05 to 0.57), which is beneficial to distinguishing small pH changes during practical applications. The curve was well fitted according to equation 3 using the two–state model, and the apparent pK_a of the nanosensors was determined to

be 4.5. The use of Equation (2) cannot fit the curve as it only suits the case of single probe (Figure S4 in the Supporting Information).

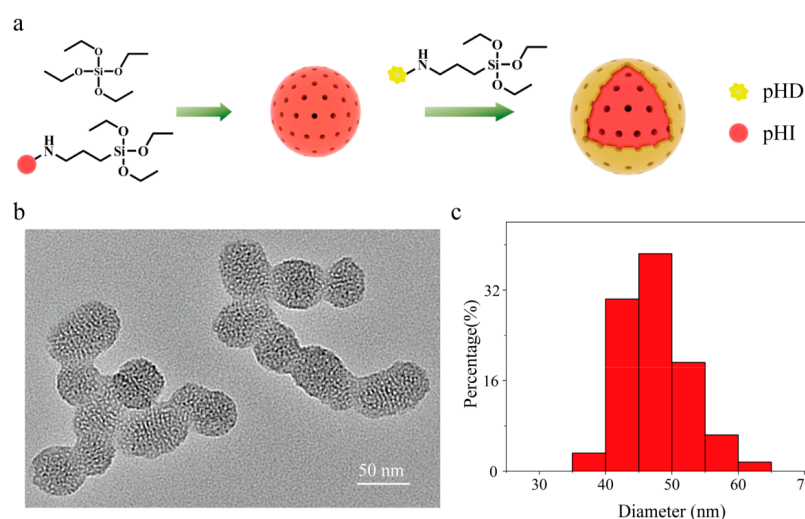


Figure 4. (a) The synthetic route, (b) the transmission electron microscopic image, and (c) the size distribution of the ratiometric pH nanosensors.

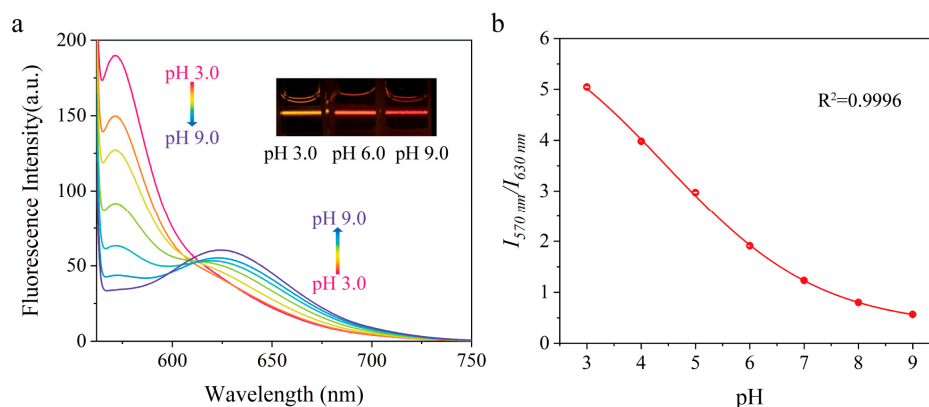


Figure 5. (a) The fluorescence emission spectra of the nanosensors in BR buffer solution at different pH values. the insert: photograph of nanosensors in BR buffer solution at different pHs under 532 nm laser pointer. (b) pH–dependent emission intensity ratio of the nanosensors at 570 nm and 630 nm.

The densely immobilized probes have excellent photostability. The suspension of nanosensors was subjected to continuously illuminating at 545 nm for 1 h. Results shown in Figure 6a illustrated that the fluorescence intensity at 570 nm decreased by 6% and that at 630 nm decreased by 5%. $I_{570\text{ nm}}/I_{630\text{ nm}}$ kept at almost a constant value (from 5.08 decline to 5.02) during the whole experiment, which ensured that error caused by the difference in probe photobleaching rate could be ignored in long–time measurement. The nanosensors maintained good photostability in solutions with varies ionic strengths (Supporting Information, Figure S5), which further extends its applications. The nanosensors showed reversible response to pH. Concentrated HCl and NaOH solution was used to switch solution pH. $I_{570\text{ nm}}/I_{630\text{ nm}}$ reached the initial values in 3 cycles, indicating the good reversibility of the nanosensors (Figure 6b and Figure S6 in the Supporting Information).

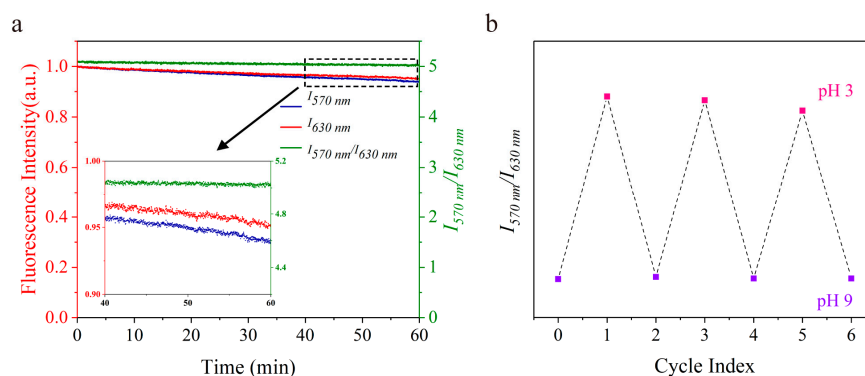


Figure 6. The photostability and reversibility of the nanosensors. (a) The nanosensors were in BR buffer (pH = 3). The fluorescence intensity was normalized. (b) The solution of nanosensors in continuous sensing of 1 M HCl/NaOH for three cycles.

Table 1 shows the comparison of our nanosensors with reported ratiometric nanosensors, they are arranged in ascending order of maximum signal intensity ratio in the fifth column.

Table 1. Ratiometric nanosensors based on two probes with opposite pH–responding direction.

Entry	$\lambda_{em\ 1}$	$\lambda_{em\ 2}$	λ_{ex}	Intensity Ratio	pH Range	Ref
1	525 nm (QDs)	605 nm (QDs)	400 nm	1.5	0.2–1.23	[20]
2	530 nm (SNARF)	630 nm (CdSe/ZnS QDs)	365 nm	3.1	6–8	[21]
3	421 nm (anthracene)	580 nm (rhodamine)	364 nm	4.1	3.73–8.11	[22]
4	470 nm (PyMMP)	630 nm (CdSe/ZnS QDs)	365 nm	5.4	1–5	[23]
5	520 nm (ITK carboxyl QDs)	560 nm (mOrange)	400 nm	8	6.1–8	[24]
6	518 nm (FITC)	575 nm (RhBAM)	488 nm	8.3	3–6	[12]
7	500 nm (Coumarin 6)	620 nm (Nile Red)	450 nm	8.75	5–9	[25]
8	520 nm (carboxyl–functionalized QDs)	560 nm (mOrange/mOrange M163K)	400 nm	12	6–8	[26]
9	570 nm (pHD)	630 nm (pHI)	545 nm	9	3–9	this work

Obviously, the excitation wavelength of our nanosensors is the longest among the nanosensors, accompanied by the longest emission wavelengths. In addition, the designed nanosensors has merits in terms of signal intensity ratio and pH measurement range. The reported ratiometric nanosensors have small signal intensity ratio or limited measurement range. Last but not the least, the nanosensors possessed advantageous photostability compared to others. Take entry 5–9 for example whose signal intensity ratio are close to each other. As for entry 5 and 8, signal intensity ratio declined by 90% and 60% after 30 min of continuous illumination, respectively [26]. As for entry 6, poor photostability of FITC hinders its application for long–term pH sensing as mentioned above [2,12,13]. As for entry 7, the pH–sensing capability relies on the introduction of pH indicator BTB, so the leakage of BTB brought error in the signal intensity ratio [25]. In conclusion, our ratiometric pH–sensitive nanosensors were superior in sensitivity, accuracy, and stability to the reported ratiometric nanosensors.

Finally, the nanosensors were applied to measure the pH values of colored aqueous samples, including polluted water, tap water, and Coca Cola. The obtained data were verified using pH test stripes and classic pH electrode. As summarized in Figure 7, the measured pH values using the nanosensors correlated well with that of pH electrodes. Considering the possible higher level of heavy metal ions in aqueous samples, we further studied the influences of heavy metal ions on sensor performance. As shown in Figure S7 in the supporting information, the interferences of Ba (II), Co (II), and Zn (II) ions on sensor signal can be ignored. In the case of Cu (II) and Fe (III) ions, the intensity ratio slightly lower

compared with control, which is attribute to their intense color [27,28]. The presence of Sn (II) ion caused increases in fluorescence intensity ratio, which was due to the hydrolysis of Sn (II) ion induced pH decreases. It should be mentioned that the concentrations of all tested heavy metal ions ($50 \text{ mg}\cdot\text{L}^{-1}$) remarkably exceed that allowed by Integrated Wastewater Discharge Standard of China [29]. Therefore, due to superior feature of long wavelength excitation and emission, the nanosensors are able to accurately measure pH values of strong colored samples, such as polluted river water and Coca Cola, which proves the measurement accuracy of the nanosensors in complicate samples.

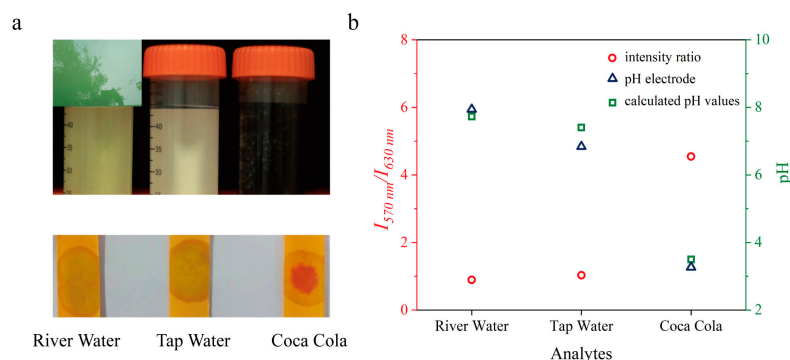


Figure 7. Determination of pH values in aqueous samples using the pH nanosensors. (a) Top: pictures of the tested samples, from left to right: river water, tap water, and Coca Cola. Bottom: pH determination using pH test stripes. (b) pH values determined using the nanosensors and pH electrode.

4. Conclusions

We have constructed highly photostable ratiometric pH-sensitive nanosensors. The opposite pH-responding direction of the two probes was conducive to improving the sensitivity of the nanosensors. The porous structure of mSiNPs made protons easily diffuse inside and interact with both dyes. The obtained nanosensors exhibited near nine-fold signal ($I_{570 \text{ nm}}/I_{630 \text{ nm}}$) change between pH 3.0 and 9.0. The constructed nanosensors showed good photostability and reversibility and were able to measure pH values in complicated samples, which are suitable for long-term monitoring of pH variation.

Supplementary Materials: The following supporting information can be downloaded at: <https://www.mdpi.com/article/10.3390/chemosensors10090354/s1>, Figure S1: The transmission electron microscopic image and fluorescence spectra of pHI@SiO₂ (prepared by method C—the method used in the manuscript); Figure S2: The transmission electron microscopic image and fluorescence spectra of pHI@SiO₂; Figure S3: The pH responses of pHI@mSiO₂—pHD synthesized with different molar ratio of pHI and pHD; Figure S4: pH-dependent fluorescence intensity ratio $\frac{I - I_{min}}{I_{max} - I}$ of the nanosensors, the curve was fitted according to Equation (2), which cannot describe the response of the nanosensor; Figure S5: The photostability of the nanosensors in the solution with various ionic strengths; Figure S6: The reversibility of the nanosensors; Figure S7: Fluorescence intensity ratio ($I_{570 \text{ nm}}/I_{630 \text{ nm}}$) of nanosensors in the presence of various heavy metal ions at a concentration of $50 \text{ mg}\cdot\text{L}^{-1}$; Table S1: Optimization of molar ratios of pHI and pHD immobilized in the nanosensors.

Author Contributions: Conceptualization, X.-D.W.; experimental work, Z.L. and F.H.; writing—original draft preparation, Z.L.; writing—review and editing, G.H., Y.Y., Y.L., X.L. and X.-D.W.; project administration, X.-D.W. All authors have read and agreed to the published version of the manuscript.

Funding: This research was funded by Shanghai Municipal Science and Technology Major Project (Grant No. 2017SHZDZX01) and the National Science Foundation of China (Grant No. 21775029).

Institutional Review Board Statement: Not applicable.

Informed Consent Statement: Not applicable.

Data Availability Statement: Not applicable.

Conflicts of Interest: The authors declare no conflict of interest.

References

1. Khan, M.I.; Mukherjee, K.; Shoukat, R.; Dong, H. A review on pH sensitive materials for sensors and detection methods. *Microsyst. Technol.* **2017**, *23*, 4391–4404. [[CrossRef](#)]
2. Steinegger, A.; Wolfbeis, O.S.; Borisov, S.M. Optical sensing and imaging of pH values: Spectroscopies, materials, and applications. *Chem. Rev.* **2020**, *120*, 12357–12489. [[CrossRef](#)] [[PubMed](#)]
3. Zhang, Y.L.; Ding, L.J.; Zhang, W.; Zhang, X.A.; Lian, Y.; Wang, X.D. A background–subtraction strategy leads to ratiometric sensing of oxygen without recalibration. *Analyst* **2018**, *143*, 5120–5126. [[CrossRef](#)]
4. Zhang, Z.J.; Seitz, W.R. A fluorescence sensor for quantifying pH in the range from 6.5 to 8.5. *Anal. Chim. Acta.* **1984**, *160*, 47–55. [[CrossRef](#)]
5. Parker, J.W.; Laksin, O.; Yu, C.; Lau, M.L.; Klima, S.; Fisher, R.; Scott, I.; Atwater, B.W. Fiberoptic sensors for pH and carbon–dioxide using a self–referencing dye. *Anal. Chem.* **1993**, *65*, 2329–2334. [[CrossRef](#)]
6. Miesenbock, G.; De Angelis, D.A.; Rothman, J.E. Visualizing secretion and synaptic transmission with pH–sensitive green fluorescent proteins. *Nature* **1998**, *394*, 192–195. [[CrossRef](#)] [[PubMed](#)]
7. Beneto, A.J.; Thiagarajan, V.; Siva, A. A tunable ratiometric pH sensor based on phenanthro[9,10–d]imidazole covalently linked with vinylpyridine. *RSC Adv.* **2015**, *5*, 67849–67852. [[CrossRef](#)]
8. Bishnoi, S.; Milton, M.D. Tunable phenothiazine hydrazones as color displaying, ratiometric and reversible pH sensors. *Tetrahedron Lett.* **2015**, *56*, 6633–6638. [[CrossRef](#)]
9. Chen, Y.; Zhu, C.; Cen, J.; Bai, Y.; He, W.; Guo, Z. Ratiometric detection of pH fluctuation in mitochondria with a new fluorescein/cyanine hybrid sensor. *Chem. Sci.* **2015**, *6*, 3187–3194. [[CrossRef](#)]
10. Lee, M.H.; Han, J.H.; Lee, J.H.; Park, N.; Kumar, R.; Kang, C.; Kim, J.S. Two–color probe to monitor a wide range of pH values in cells. *Angew. Chem. Int. Ed.* **2013**, *52*, 6206–6209. [[CrossRef](#)]
11. Vasylevska, A.S.; Karasyov, A.A.; Borisov, S.M.; Krause, C. Novel coumarin–based fluorescent pH indicators, probes and membranes covering a broad pH range. *Anal. Bioanal. Chem.* **2007**, *387*, 2131–2141. [[CrossRef](#)] [[PubMed](#)]
12. Shi, P.; Liu, Z.; Dong, K.; Ju, E.; Ren, J.; Du, Y.; Li, Z.; Qu, X. A smart “Sense–Act–Treat” system. Combining a ratiometric pH sensor with a near infrared therapeutic gold nanocage. *Adv. Mater.* **2014**, *26*, 6635–6641. [[CrossRef](#)] [[PubMed](#)]
13. Peng, J.F.; He, X.X.; Wang, K.M.; Tan, W.H.; Wang, Y.; Liu, Y. Noninvasive monitoring of intracellular pH change induced by drug stimulation using silica nanoparticle sensors. *Anal. Bioanal. Chem.* **2007**, *388*, 645–654. [[CrossRef](#)] [[PubMed](#)]
14. Hu, F.; Huang, Y.X.; Xiao, Y.S.; Li, Y.C.; Luo, X.; Qian, X.H.; Yang, Y.J. A dual–channel Hill–type small–molecule pH probe. *Anal. Methods* **2021**, *13*, 3012–3016. [[CrossRef](#)]
15. Chen, W.; Xu, S.; Day, J.J.; Wang, D.F.; Xian, M. A general strategy for development of near–Infrared fluorescent probes for bioimaging. *Angew. Chem. Int. Ed.* **2017**, *56*, 16611–16615. [[CrossRef](#)]
16. Fulaz, S.; Hiebner, D.; Barros, C.H.N.; Devlin, H.; Vitale, S.; Quinn, L.; Casey, E. Ratiometric imaging of the in situ pH distribution of biofilms by use of fluorescent mesoporous silica nanosensors. *ACS Appl. Mater. Interfaces* **2019**, *11*, 32679–32688. [[CrossRef](#)]
17. Vuppu, S.; Kostov, Y.; Rao, G. Economical wireless optical ratiometric pH sensor. *Meas. Sci. Technol.* **2009**, *20*, 045202. [[CrossRef](#)]
18. Bizzarri, R.; Arcangeli, C.; Arosio, D.; Ricci, F.; Faraci, P.; Cardarelli, F.; Beltram, F. Development of a novel GFP–based ratiometric excitation and emission pH indicator for intracellular studies. *Biophys. J.* **2006**, *90*, 3300–3314. [[CrossRef](#)]
19. Bizzarri, R.; Serresi, M.; Luin, S.; Beltram, F. Green fluorescent protein based pH indicators for in vivo use: A review. *Anal. Bioanal. Chem.* **2009**, *393*, 1107–1122. [[CrossRef](#)]
20. Hiruta, Y.; Yoshizawa, N.; Citterio, D.; Suzuki, K. Highly durable double sol–gel layer ratiometric fluorescent pH optode based on the combination of two types of quantum dots and absorbing pH indicators. *Anal. Chem.* **2012**, *84*, 10650–10656. [[CrossRef](#)]
21. Somers, R.C.; Lanning, R.M.; Snee, P.T.; Greytak, A.B.; Jain, R.K.; Bawendi, M.G.; Nocera, D.G. A nanocrystal–based ratiometric pH sensor for natural pH ranges. *Chem. Sci.* **2012**, *3*, 2980–2985. [[CrossRef](#)] [[PubMed](#)]
22. Marin, M.J.; Galindo, F.; Thomas, P.; Russell, D.A. Localized intracellular pH measurement using a ratiometric photoinduced electron–transfer–based nanosensor. *Angew. Chem. Int. Ed.* **2012**, *51*, 9657–9661. [[CrossRef](#)] [[PubMed](#)]
23. Paek, K.; Chung, S.; Cho, C.-H.; Kim, B.J. Fluorescent and pH–responsive diblock copolymer–coated core–shell CdSe/ZnS particles for a color–displaying, ratiometric pH sensor. *Chem. Commun.* **2011**, *47*, 10272–10274. [[CrossRef](#)] [[PubMed](#)]
24. Dennis, A.M.; Bao, G. Quantum dot–fluorescent protein pair as ratiometric pH sensor. *Proc. SPIE* **2010**, *7575*, 45–53. [[CrossRef](#)]
25. Peng, H.S.; Stolwijk, J.A.; Sun, L.N.; Wegener, J.; Wolfbeis, O.S. A nanogel for ratiometric fluorescent sensing of intracellular pH values. *Angew. Chem. Int. Ed.* **2010**, *49*, 4246–4249. [[CrossRef](#)] [[PubMed](#)]
26. Dennis, A.M.; Rhee, W.J.; Sotto, D.; Dublin, S.N.; Bao, G. Quantum dot–fluorescent protein FRET probes for sensing intracellular pH. *ACS Nano* **2012**, *6*, 2917–2924. [[CrossRef](#)]
27. Liang, Y.H.; Deng, R.R.; Gao, Y.K.; Qin, Y.; Liu, X.L. Measuring absorption coefficient spectrum (400–900 nm) of copper ions in water. *J. Remote Sens.* **2016**, *20*, 27–34. [[CrossRef](#)]
28. Deng, R.R.; Liang, Y.H.; Gao, Y.K.; Qin, Y.K.; Lin, X.L. Measuring absorption coefficient spectrum (400–900 nm) of hydrated and complex ferric ion in water. *J. Remote Sens.* **2016**, *20*, 35–44. [[CrossRef](#)]
29. GB 8978–1996; Integrated Wastewater Discharge Standard of China. Ministry of Environmental Protection of the People’s Republic of China: Beijing, China, 1996.